Effect of *s-d* Interaction on the Spin-Lattice Relaxation in Dilute Magnetic Alloys

N. Menyhård and F. Sólyom
Central Research Institute for Physics, Budapest, Hungary
and
A. Zawadowski*†
Department of Physics, University of Virginia, Charlottesville, Virginia 22903
(Received 24 February 1970)

The contributions of magnetic impurities to the conduction-electron–lattice and impurity-spin–lattice relaxation rates (T_{sl}^{-1} and T_{dl}^{-1}, respectively) are theoretically investigated. The conduction-electron-impurity interaction is described by a Kondo *s-d* exchange Hamiltonian with scattering of *d* type. It is assumed that in the absence of *s-d* exchange interaction there are direct lattice relaxation processes ($T_{sl}^{(0)-1}$ and $T_{dl}^{(0)-1}$) which are introduced in a phenomenological way, since the detailed mechanism of the *d*-electron–lattice relaxation is not known. As the *s-d* exchange interaction is relatively strong compared to the lattice relaxation processes, the contribution of a magnetic impurity to the relaxation rates can be essentially modified by the *s-d* interaction associated with the same impurity. The calculations are performed treating only the leading logarithmic terms in any order of the perturbation theory. This approximation limits the adequacy of the result to the regime well above the Kondo temperature and demonstrates the appearance and features of the Kondo effect in the lattice relaxation processes. However, a theory which covers the whole temperature range correctly is very likely not available at the present stage of the theory of the Kondo effect. It is found that the conduction-electron–lattice relaxation is depressed, which may be interpreted as the result of the change in the density of conduction electrons at the Fermi energy. The impurity-spin–lattice relation is found to be enhanced (depressed) for $S > \frac{1}{2}$ ($S = \frac{1}{2}$). These renormalizations exhibit a strong temperature dependence in the region of the Kondo temperature which may be of importance in the interpretation of the recent transmission electron-spin-resonance experiments.

I. INTRODUCTION

In the last few years numerous theoretical and experimental investigations have been performed to explain the behavior of magnetic impurities in dilute alloys. The basic problem is whether a spin-compensated state (Kondo state) is formed around the impurity atom or not. This problem can be attacked experimentally by measuring both the static and dynamic properties, e.g., the relaxation processes. Recently, the application of the transmission electron-spin-resonance (TESR) technique to the investigation of dilute alloys has been reported by several authors.[1-3] In this method the resonance signal due to the impurity atoms can be detected. The phenomenological theory of TESR has been developed by Hasegawa[4] and later generalized by Schultz *et al.*[2,3] They supposed that not only the conduction-electron spin relaxes to the lattice (with relaxation rate T_{sl}^{-1}), but also the local moment relaxes with relaxation rate T_{dl}^{-1}. Phenomenologically they have assumed that these quantities are independent of temperature and could fit rather well the experimental data on Cr or Mn impurities in Cu host.

The conduction-electron–lattice relaxation due to the magnetic impurities and the impurity-spin–lattice relaxation take place in the neighborhood of the impurities. Since the lattice relaxation is weaker than the exchange interaction between the conduction electron and the localized spin, the latter interaction must modify the lattice relaxation rate. The *s-d* interaction is especially strong in the region of the Kondo temperature and below it, where conduction-electron scattering on the impurity spin shows a resonant behavior in the neighborhood of the Fermi energy. The temperature interval in which the measurements have been performed lies in the neighborhood of the Kondo temperature, and therefore it can be expected that the Kondo effect has strong influence on T_{sl} and T_{dl} and leads to a temperature-dependent correction.

It is the aim of the present paper to investigate the effect of the Kondo scattering on the relaxation rates mentioned before by calculating the renormalization due to the Kondo *s-d* interaction (H_{sd}) of the transition probabilities for such processes in which either the conduction-electron spin changes and the local moment is conserved or reversed. The interaction causing the relaxation of the conduction-electron spins to the lattice is the spin-orbit interaction of *s* electrons in the impurity potential (H_{sl}). The mechanism of the local-moment–lattice relaxation is, however, not clear and no explicit form for the local-moment–lattice interaction (H_{dl}) is available.[5,6] In the present paper a simple phenomenological form will be

assumed for the local-moment–lattice relaxation that describes the transfer of the moment to the lattice.

We have calculated the relaxation rate T_{sl}^{-1} taking into account H_{sl} and H_{sd}, as well as T_{dl}^{-1} with the help of H_{dl} and H_{sd}. We find that in the neighborhood of the Kondo temperature the temperature-dependent corrections cannot be neglected and with decreasing temperature T_{sl}^{-1} decreases, while T_{dl}^{-1} increases if $S > \frac{1}{2}$, and vice versa for $S = \frac{1}{2}$. Furthermore, there is a contribution to T_{dl}^{-1} coming from the H_{sl} vertex renormalized by the s-d interaction. This contribution, however, as will be shown, can be neglected at low temperatures compared to the other part of T_{dl}^{-1}. Similarly, a formal calculation shows that H_{dl} might contribute to T_{sl}^{-1}; unfortunately, this contribution diverges. In fact, the effect of H_{dl} cannot be taken into account by applying the perturbation theory for these processes, and so it is beyond the scope of the present paper.

In Sec. II we describe the model to be investigated. The Hamiltonian of the system is given as well as the elements of the special diagrams used to represent the different processes in the transition probability. The renormalization of T_{sl} and T_{dl} is treated in Secs. III and IV, respectively. First the transition probability is calculated up to second order in the coupling constant of the s-d interaction and then it is generalized to higher orders in logarithmic approximation. In Sec. V we summarize and discuss the results obtained.

II. FORMULATION OF PROBLEM

We investigate the relaxation of the total magnetization in a system, where magnetic impurities are imbedded in a metallic host (e.g., Cr ions in Cu). It is supposed that the electrons interact with the magnetic moment of the impurities via an s-d exchange interaction and that the impurity potential gives rise to a spin-orbit interaction for the scattered electrons. Schultz *et al.*[2] have shown that the direct relaxation of the local moment to the lattice is in great part responsible for the behavior of the Cu(Cr) alloy at low temperatures. Therefore we have to add also this interaction H_{dl} to the Hamiltonian.

The total Hamiltonian of the system is

$$H = H_0 + H' = H_0 + H_{sd} + H_{sl} + H_{dl} \quad . \tag{1}$$

The first term

$$H_0 = \sum_{\vec{k},\alpha} \epsilon_{\vec{k}\alpha} a_{\vec{k}\alpha}^{\dagger} a_{\vec{k}\alpha} \tag{2}$$

is the kinetic energy of the conduction electrons, $a_{\vec{k}\alpha}$ ($a_{\vec{k}\alpha}^{\dagger}$) is the annihilation (creation) operator of an electron with momentum $\vec{k}$ and spin direction α.

The s-d interaction term is written in the form[7]

$$H_{sd} = -\sum_{\vec{k},\vec{k}',n;l,\alpha,\beta} (2l+1)\,(J_l/N)\,P_l(\cos\theta_{\vec{k}\vec{k}'}) \times e^{i(\vec{k}'-\vec{k})\cdot\vec{R}_n} \vec{S}_n\, a_{\vec{k}\alpha}^{\dagger} \vec{\sigma}_{\alpha\beta}\, a_{\vec{k}'\beta} \quad , \tag{3}$$

where J_l is the coupling constant of the interaction for the lth partial wave, N is the number of atoms in the crystal, $\vec{S}_n$ is the spin operator of the impurity at position $\vec{R}_n$, σ denotes the Pauli matrix, $P_l(x)$ means the lth Legendre polynomial, and $\theta_{\vec{k}\vec{k}'}$ is the angle between the conduction-electron momenta $\vec{k}$ and $\vec{k}'$. Usually the momentum dependence of J is taken into account by a cutoff at some value of $|k|$ and $|k'|$, but the angular dependence is neglected. In the present case, however, such an approximation would not lead to any renormalization of T_{sl}. It will be supposed that the dominant contribution comes from the $l = 2$ part, since the impurities are $3d$ transition elements. For rare-earth impurity atoms $l = 3$.[8] Instead of J_2, the notation J will be used.

Supposing that the electron-orbit–lattice relaxation is much stronger than the relaxation of the conduction-electron spin to the orbit, the spin-lattice interaction can be represented by a spin-orbit potential[9] acting on the electrons in the vicinity of the impurities:

$$H_{sl} = -i\sum_{\vec{k},\vec{k}',n;l,\alpha,\beta} \frac{B_l}{N} e^{i(\vec{k}'-\vec{k})\vec{R}_n} P_l^1(\cos\theta_{\vec{k}\vec{k}'}) \times \frac{\vec{k}\times\vec{k}'}{|\vec{k}\times\vec{k}'|}\, a_{\vec{k}\alpha}^{\dagger} \vec{\sigma}_{\alpha\beta}\, a_{\vec{k}'\beta} \quad , \tag{4}$$

where B_l is the coupling constant of this interaction and can be expressed with the help of the phase shift, and $P^1(x)$ is the associated Legendre polynomial. It can be shown that in the present calculation it is sufficient to keep only the $l = 2$ term in the spin-orbit interaction as well. In fact all odd-l terms give no contribution, and all even-l terms contribute similarly to that of the $l = 2$ term; thus we may keep only $l = 2$.

Furthermore, for the local-moment–lattice interaction we assume

$$H_{dl} = -\sum_n (A^z S_n^z + A^+ S_n^- + A^- S_n^+) \, , \tag{5}$$

where A^z, $A^{\pm}$ can be treated as operators acting in the space of the lattice wave functions. The matrix elements of $A^{\pm}$ between the initial and final states of the lattice (which are unknown for us), determine the unrenormalized $T_{dl}^{(0)-1}$. In the calculation of the renormalization factor connecting T_{dl}^{-1} with $T_{dl}^{(0)-1}$, these matrix elements are irrelevant if the energy transfer to the lattice is of the order of the thermal energy or less. For the sake of simplicity, these matrix elements can be supposed to be independent of the lattice quantum numbers.

Therefore, in the following $A^+ = (A^-)^*$ will denote these matrix elements as phenomenological constants.

In the following we will always restrict the investigations to the one-impurity problem, that is, we suppose that the spin-orbit and s-d interactions take place on the same impurity. The contributions nonlinear in the impurity concentration will be neglected.

In order to obtain T_{sl}^{-1} and T_{dl}^{-1}, we have to calculate the transition probability between the initial state $|i\rangle$ and final state $|f\rangle$ with the help of the golden rule

$$W_{i\to f} = 2\pi |R_{fi}|^2 \delta(E_i - E_f), \tag{6}$$

where $R_{fi} = \langle f|R|i\rangle$ and

$$R = H' + H'(E_i - H_0 + i\delta)^{-1} R. \tag{7}$$

Two relaxation processes are to be considered. In the conduction-electron spin-lattice relaxation (T_{sl}), the initial and final states are

$$|i\rangle = |\vec{k}\uparrow, M\rangle \text{ and } |f\rangle = |\vec{k}'\downarrow, M\rangle, \tag{8}$$

where $|\vec{k}\uparrow\rangle$ denotes the Fermi sea with an excess spin-up electron of momentum $\vec{k}$, and M is the z component of the impurity spin. In this process the conduction electron scattered off the impurity changes its spin direction.

For the other process, called local-moment–lattice relaxation (T_{dl}), we have

$$|i\rangle = |\vec{k}\uparrow, M\rangle, \quad |f\rangle = |\vec{k}'\uparrow, M-1\rangle \tag{9}$$

or

$$|i\rangle = |\vec{k}\downarrow, M\rangle, \quad |f\rangle = |\vec{k}'\downarrow, M-1\rangle. \tag{10}$$

Since the spin-orbit and local-moment–lattice interactions can be taken to be much smaller than the s-d exchange interaction ($A, B \ll |J|$), R_{fi} will be calculated to first order in H_{sl} and H_{dl}, while the effect of H_{sd} will be included to all orders.

In order to visualize the processes, we use time-ordered diagrams. In the diagrams the time runs from the left to the right. Solid lines going to the right (left) represent the propagation of an electron (hole). The interaction vertices are shown in Fig. 1. A vertical dotted line with one incoming and one outgoing electron or hole line stands for H_{sd}, a similar vertex with a wavy line

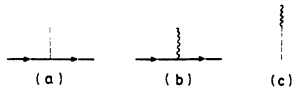

FIG. 1. Elementary vertices of the (a) s-d, (b) spin-lattice, and (c) local-moment-lattice interactions.

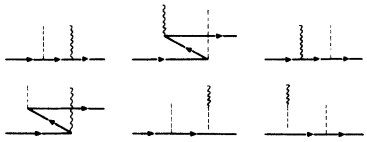

FIG. 2. Second-order diagrams of R_{fi} for the spin-lattice relaxation.

for H_{sl}. H_{dl} is represented by a vertex point with one wavy and one dotted line.

III. RENORMALIZATION OF T_{sl}

For the relaxation processes when the conduction-electron spin relaxes to the lattice, we have to take into account the initial and final states given in (8). To obtain the relaxation rate T_{sl}^{-1}, the transition probability of the inverse process must also be calculated. Unless a strong magnetic field is present, the renormalization factor of these two processes is the same as a consequence of time-reversal symmetry.

The first-order contribution of the spin-orbit interaction to R_{fi} is given by

$$R_{fi}^{(1)} = i(B/N)[(\vec{k}\times\vec{k}')^+ / |\vec{k}\times\vec{k}'|] P_2^1(\cos\theta_{\vec{k}\vec{k}'}), \tag{11}$$

where $(\vec{k}\times\vec{k}')^+ = (\vec{k}\times\vec{k}')_x + i(\vec{k}\times\vec{k}')_y$, and this contribution is represented by the diagram in Fig. 1(b).

The second-order diagrams are shown in Fig. 2. The contribution of the processes associated to H_{sl} corresponding to the first four diagrams in Fig. 2 is

$$R_{fi}^{(2)} = i\frac{BJ}{NN} 5\sum_{\vec{k}_1} P_2(\cos\theta_{\vec{k}\vec{k}_1}) M \frac{(\vec{k}_1\times\vec{k}')^+}{|\vec{k}_1\times\vec{k}'|} P_2^1(\cos\theta_{\vec{k}_1\vec{k}'})$$
$$\times\left(\frac{1-n_f(\epsilon_{\vec{k}_1})}{\epsilon_{\vec{k}}-\epsilon_{\vec{k}_1}+i\delta} + \frac{n_f(\epsilon_{\vec{k}_1})}{\epsilon_{\vec{k}}-\epsilon_{\vec{k}_1}-i\delta}\right) - i\frac{BJ}{NN}$$
$$\times 5\sum_{\vec{k}_1} \frac{(\vec{k}\times\vec{k}_1)^+}{|\vec{k}\times\vec{k}_1|} P_2^1(\cos\theta_{\vec{k}_1\vec{k}'}) P_2(\cos\theta_{\vec{k}_1\vec{k}'}) M$$
$$\times\left(\frac{1-n_f(\epsilon_{\vec{k}_1})}{\epsilon_{\vec{k}}-\epsilon_{\vec{k}_1}+i\delta} + \frac{n_f(\epsilon_{\vec{k}_1})}{\epsilon_{\vec{k}}-\epsilon_{\vec{k}_1}-i\delta}\right), \tag{12}$$

where n_f denotes the Fermi distribution function.

The contribution of the last two diagrams in Fig. 2 can be calculated in a similar way and the result is

$$A^+\frac{J}{N} 5P_2(\cos\theta_{\vec{k}\vec{k}'})\left(\frac{1}{\epsilon-\epsilon_{\vec{k}'}+i\delta}[S(S+1)-M(M+1)]\right.$$
$$\left.+\frac{1}{\epsilon_{\vec{k}}-\epsilon_{\vec{k}'}+i\delta}[S(S+1)-M(M-1)]\right).$$

However, taking into account the energy conservation $\epsilon_{\vec{k}} = \epsilon_{\vec{k}'}$, these terms diverge when $\delta \to +0$. The reason for this unphysical divergence is that there is not any energy transfer in the processes associated with H_{dl}. Therefore, these processes must be taken into account exactly by introducing the exact localized spin states in considering H_{dl}. This procedure corresponds to the summation of a large class of diagrams in the Green's-function technique. The solution of the problem would be yielded by calculating the dynamical susceptibility actually measured in experiments. Unfortunately, this calculation is a very delicate question, as will be pointed out in the discussion in Sec. V, and it is beyond the scope of the present paper. On the other hand, a direct calculation of the relaxation rate by applying the exact spin states has not been performed, since in this case we have not been able to separate the lattice relaxation processes from the conduction-electron localized-spin relaxation processes. In this way we conclude that to answer the question whether H_{dl} contributes to T_{sl}^{-1} or not requires further theoretical investigations.

In what follows we will treat only the terms first order in H_{sl} and any order in H_{sd}. In second order in J there are 24 time-ordered diagrams. Four representatives are shown in Fig. 3. All the other diagrams can be generated from them by different time ordering of the vertices. They can also be thought as Feynman diagrams,[10] where the solid line corresponds to the propagator

$$G(\epsilon_{\vec{k}_1}) = \frac{1 - n_f(\epsilon_{\vec{k}_1})}{\epsilon_k - \epsilon_{\vec{k}_1} + i\delta} + \frac{n_f(\epsilon_{\vec{k}_1})}{\epsilon_k - \epsilon_{\vec{k}_1} - i\delta} \quad . \tag{13}$$

The contribution of the last diagram is zero, as can easily be seen by calculating the angular integrals for the Legendre polynomials. The other three diagrams yield

$$R_{fi}^{(3)} = -i\frac{B}{N}\left(\frac{J}{N}\right)^2 25 \sum_{\vec{k}_1,\vec{k}_2} G(\epsilon_{\vec{k}_1}) G(\epsilon_{\vec{k}_2}) \Bigg[P_2(\cos\theta_{\vec{k}\vec{k}_1}) P_2(\cos\theta_{\vec{k}_1\vec{k}_2}) \frac{(\vec{k}_2\times\vec{k}')^*}{|\vec{k}_2\times\vec{k}'|} P_2^1(\cos\theta_{\vec{k}_2\vec{k}'}) S(S+1) - P_2(\cos\theta_{\vec{k}\vec{k}_1})$$
$$\times \frac{(\vec{k}_1\times\vec{k}_2)^*}{|\vec{k}_1\times\vec{k}_2|} P_2^1(\cos\theta_{\vec{k}_1\vec{k}_2}) P_2(\cos\theta_{\vec{k}_2\vec{k}'}) M^2 + \frac{(\vec{k}\times\vec{k}_1)^*}{|\vec{k}\times\vec{k}_1|} P_2^1(\cos\theta_{\vec{k}\vec{k}_1}) P_2(\cos\theta_{\vec{k}_1\vec{k}_2}) P_2(\cos\theta_{\vec{k}_2\vec{k}'}) S(S+1) \Bigg] . \tag{14}$$

Adding the contributions in Eqs. (11), (12), and (14) and calculating the transition probability up to terms of order $(BJ)^2$ (after averaging over the directions of $\vec{k}$ and $\vec{k}'$, and over the value of M), a straightforward but tedious calculation gives

$$|\tilde{R}_{fi}|^2 = \tfrac{4}{5}(B/N)^2\{1 - \tfrac{10}{3} S(S+1)\pi^2(J\rho_0/N)^2$$
$$\times [1 - 2n_f(\epsilon_{\vec{k}})]^2 + \cdots\} , \tag{15}$$

where ρ_0 is the density of states of conduction electrons at the Fermi surface and the bar above $|R_{fi}|^2$ denotes that the averages have been performed.

Here it should be noticed that the integrals of the type

$$\sum_{\vec{k}_1} P/(\epsilon - \epsilon_{\vec{k}_1}) ,$$

where P stands for the principal value, have been neglected. This is an approximation usually used.[11]

For temperatures lying in the vicinity of the Kondo temperature, one must go beyond this approximation and corrections of higher order in J have to be taken into account. In the upper neighborhood of the Kondo temperature this will be done in logarithmic approximation. The details of the calculation show that the main contribution to $|R_{fi}|^2$ comes from a certain class of diagrams. In third order such diagrams are those shown in Figs. 3(a) and 3(c) and the contribution of the H_{sl} vertex renormalization [Fig. 3(b)] is canceled by the cross product of the two second-order contributions. This feature of the contributions of the various diagrams persists in every order to logarithmic accuracy, as will be shown in the Appendix. Consequently, this approximation to the square of the transition matrix element consists in replacing $(J/N)^2\rho_0\pi S(S+1)$ in the second term in Eq. (15) by the renormalized self-energy[12] of the conduction electrons. Thus we get

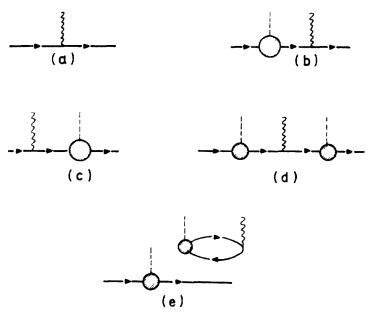

FIG. 3. Third-order diagrams of R_{fi} for the spin-lattice relaxation.

$$|\bar{R}_{fi}|^2=\frac{4}{5}\left(\frac{B}{N}\right)^2\left\{1-\frac{10}{3}S(S+1)\pi^2\left(\frac{J\rho_0}{N}\right)^2 \times \frac{[1-2n_f(\epsilon_{\vec{k}})]^2}{[1+2(J\rho_0/N)\ln(D/T)]^2}\right\} \quad (16)$$

for $T \gg T_K$, where D is the cutoff energy generally used in the Kondo problem, and T_K denotes the Kondo temperature.

In order to obtain the renormalization factor of the relaxation rate $1/T_{s1}$, $|R_{fi}|^2$ has to be averaged over the incoming and outgoing electron energies, taking into account the Fermi distribution functions $n_f(\epsilon_k)$ and $1-n_f(\epsilon_{k'})$, respectively. Using the relation

$$\frac{\int[1-2n_f(\epsilon_k)]^2\{n_f(\epsilon_k)[1-n_f(\epsilon_k)]\}\,d\epsilon_k}{\int\{n_f(\epsilon_k)[1-n_f(\epsilon_k)]\}\,d\epsilon_k}=\frac{1}{3}\ , \quad (17)$$

finally for $T \gg T_K$ we obtain

$$\frac{1}{T_{s1}}=\frac{1}{T_{s1}^{(0)}}\left[1-\tfrac{10}{9}S(S+1)\pi^2\left(\frac{J\rho_0}{N}\right)^2 \times [1+2(J\rho_0/N)\ln(D/T)]^2\right]. \quad (18)$$

It is worth mentioning that the decrease of the renormalization factor in Eq. (18) with decreasing temperature is closely connected with the decrease of the density of states around a magnetic impurity at low temperatures[13] which gives rise to the zero bias anomalies in doped tunnel junctions as well.[14] Namely, it can be shown[13] that as a result of the interference between the incoming and outgoing conduction-electron scattering waves, the electron density is depressed at the impurity site in the neighborhood of Fermi energy and the measure of this depression is proportional to the imaginary part of electron self-energy. Actually, the diagrams in Figs. 3(a) and 3(c) provide a renormalization of the relaxation rate which contains the imaginary part of the self-energy. If the density of states is depressed around the impurity, the probability of the spin-orbit relaxation has to be reduced, as is found.

Below the Kondo temperature an equation of Chew-Low type[15] ought to be solved to obtain a temperature dependence for low temperature, for example, as has been done by Brenig and Götze[16] for the original Kondo problem. We are not going to extend our work in this direction because the solution of this type does not describe the real temperature dependence of the electrical resistivity; therefore, one can not expect to get the correct temperature dependence for this more difficult problem.

IV. RENORMALIZATION OF T_{d1}

The initial and final states of the relaxation of the local moment to the lattice are given in (9) and (10). The two cases, $\vec{k} \neq \vec{k}'$ and $\vec{k}=\vec{k}'$, have to be treated separately. In the present problem the contribution of the nonforward scattering is of no importance owing to the following reason. In calculating the relaxation rate of the local moment, the initial and final states of the conduction-electron system must be averaged over. Because of the appearance of the Fermi functions $n_f(\epsilon_k) \times [1-n_f(\epsilon_{k'})]$, this contribution is proportional to the temperature and can thus be neglected at low temperatures compared to the contribution of the forward scattering.

In the elastic channel, the first-order contribution is represented by the elementary H_{d1} vertex in Fig. 1(c) and its contribution is

$$R_{fi}^{(1)}=A^+[S(S+1)-M(M-1)]^{1/2}. \quad (19)$$

The second-order diagrams are given in Fig. 4. Their contribution is equal to zero. The first diagram gives zero owing to the integral over the angles as does the diagram in Fig. 3(d). It can be easily shown that all the diagrams of first order in H_{s1} and of any order in H_{sd} give zero contribution. Furthermore, the contribution of the second diagram in Fig. 4 is proportional to the conduction-electron spin polarization $\rho\uparrow-\rho\downarrow$, which, in the absence of an external magnetic field, is zero.

The third-order diagrams left are given in Fig. 5. The contribution of the first and third diagrams being imaginary, it does not appear in the transition probability up to second order in J. The second diagram gives, after taking into account all the possible spin orientations in the intermediate states,

$$R_{fi}^{(3)}=-A[S(S+1)-M(M-1)]^{1/2}\,50[S(S+1)-1] \times (J/N)^2\sum_{\vec{k}_1,\vec{k}_2}\frac{n_f(\epsilon_{\vec{k}_1})[1-n_f(\epsilon_{\vec{k}_2})]}{(\epsilon_{\vec{k}_1}-\epsilon_{\vec{k}_2}+i\delta)^2} \times P_2(\cos\theta_{\vec{k}_1\vec{k}_2})P_2(\cos\theta_{\vec{k}_2\vec{k}_1}). \quad (20)$$

In logarithmic approximation,

$$\sum_{\vec{k}_1,\vec{k}_2}\frac{n_f(\epsilon_{\vec{k}_1})[1-n_f(\epsilon_{\vec{k}_2})]}{(\epsilon_{\vec{k}_1}-\epsilon_{\vec{k}_2}+i\delta)^2}\approx\rho_0^2\ln\frac{D}{T}\ , \quad (21)$$

and Eq. (20) yields

$$R_{fi}^{(3)}=-A[S(S+1)-M(M-1)]^{1/2}$$

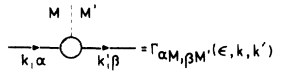

FIG. 4. Second-order diagrams of R_{fi} for the local-moment-lattice relaxation.

$$\times 10[S(S+1)-1](J\rho_0/N)^2\ln(D/T)\ . \qquad (22)$$

For the transition probability, we obtain

$$W \approx A^2[S(S+1)-M(M-1)]$$
$$\times\{1+20[S(S+1)-1](J\rho_0/N)^2\ln(D/T)\}. \qquad (23)$$

In summing up the higher-order contributions in logarithmic approximation, we use the result by Zawadowski and Fazekas[17] who have investigated a similar renormalization of the s-d vertex. It has been found to be related to the Abrikosov's pseudofermion[12] self-energy by an identity of Ward type. This self-energy has been calculated[18] with logarithmic accuracy. In this way, the result can be obtained by multiplying the second-order term by the factor $[1+2J/N\rho_0\ln(D/T)]^{-1}$. Thus we get

$$W \approx A^2[S(S+1)-M(M-1)]$$
$$\times\left(1+20[S(S+1)-1]\frac{(J\rho_0/N)^2\ln(D/T)}{1+2(J/N)\rho_0\ln(D/T)}\right) \qquad (24)$$

for $T \gg T_K$. It is worth noticing that, contrary to the renormalization of T_{sl}^{-1}, here only the first power of the typical logarithmical denominator appears.[19] According to the results of Ref. 17, for $T > T_K$ the renormalized gyromagnetic factor g_{eff} describes the magnetic screening of the impurity moment by the polarization of the conduction electrons. For the partial waves with $l=2$, the generalized result is

$$g_{eff} = g\left[1-\frac{10(J\rho_0/N)^2\ln(D/T)}{1+2(J/N)\rho_0\ln(D/T)}\right]\ . \qquad (25)$$

The relaxation rate T_{dl}^{-1} can be written in the form

$$\frac{1}{T_{dl}} = \frac{1}{T_{dl}^{(0)}}\left(1+2\,[S(S+1)-1]\,\frac{g-g_{eff}(T)}{g}\right)\ . \qquad (26)$$

Equation (24) shows that the renormalization factor for $1/T_{dl}$, as opposed to that of $1/T_{sl}$, increases with decreasing temperature for $S > \frac{1}{2}$, showing the trend indicated by the experiments. This point will be further expanded in Sec. V.

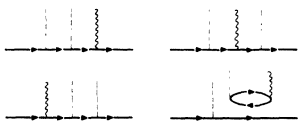

FIG. 5. Third-order diagrams of R_{fi} for the local-moment-lattice relaxation.

V. DISCUSSION

In the present paper we have investigated theoretically the effect of the s-d interaction on the conduction-electron–lattice and localized-spin–lattice relaxation rate supposing that all of these processes are induced by the same magnetic impurity. The calculations are performed in second order in the lattice relaxation rate and up to any order in the exchange coupling J by considering a certain class of diagrams. The presence of the exchange interaction is found to be effective in changing the relaxation rates. In the processes of higher order (in third order for T_{sl}^{-1} and in second order for T_{dl}^{-1}), logarithmic expressions occur which characterize the Kondo effect.[19] By summing up those diagrams which contribute up to the highest power of the logarithmic term in any order in the perturbation theory, the relaxation rates have been determined.

The temperature dependence of the relaxation processes are obtained as well, and it is found that the calculations are valid only above the Kondo temperature since an unphysical divergence appears at the Kondo temperature in the vertex function. Below and in the narrow neighborhood of the Kondo temperature, more accurate calculations are needed whose accuracy is beyond the leading logarithmic terms treated here.

Furthermore, it is shown that the conduction-electron–lattice interaction given by H_{sl} cannot contribute to the localized-spin–lattice relaxation, because of the different angular dependence of the s-d and conduction-electron–lattice interactions. Unfortunately, in the framework of the perturbation theory it is not possible to decide whether the localized-spin–lattice interaction gives rise to the conduction-electron–lattice relaxation processes or not.

Nevertheless, the present theoretical treatment unambiguously indicates that the effect of the s-d interaction on the different lattice relaxation processes is important and contributes to an additional temperature dependence of the relaxation. The results given by Eqs. (18) and (24) can be compared with experimental results for $T > T_K$. On the other hand, the structure of the expressions shows that the corrections expected for low temperature ($T < T_K$) are of the same order as the unrenormalized relaxation rate.

The result for T_{sl}^{-1} given by Eq. (18) shows that the s-d interaction reduces the conduction-electron–lattice relaxation rate as the temperature is decreased. Furthermore, it is pointed out that the depression of the conduction-electron density of states[12] at the Fermi energy in the neighborhood of the magnetic impurity is responsible (at least in part) for this reduction. However, the localized-spin–lattice relaxation rate can be increased by

lowering the temperature for $S > \frac{1}{2}$, while the effect is just the opposite for $S = \frac{1}{2}$.

For experimental study, the Cu(Cr) and Cu(Fe) systems seem to be the most appropriate for comparison to the present work. From measurements of the electrical resistivity,[20] susceptibility, and specific heat,[21] it is known that the Kondo temperature of a dilute Cu(Cr) alloy is about 1 °K. This system has already been investigated by applying the TESR technique down to 1 °K, which is near but above T_K. The electrical resistivity measurements indicate that $S = \frac{3}{2}$. The TESR data have been interpreted by Monod-Schultz[3] terms of the temperature dependence of the static susceptibilities corresponding to the electrons (X_s) and to the localized spins (X_d), quantities which occur in the formulas of the linewidth and line shape of the detected signals. Furthermore, these experimental results support the existence of a direct localized-spin–lattice relaxation channel. According to Eq. (26), for $S = \frac{3}{2}$, the T_{ds}^{-1} should increase with decreasing temperature and an enhancement of the effective relaxation rate T_{eff}^{-1}[22] by a factor of ~2 should be expected. This estimate is achieved on the basis of Eq. (26) using the values $S = \frac{3}{2}$ and $g_{eff}/g \sim 0.8$ at $T \gtrsim T_K$. However, a precise comparison of the experimental results with the theory would be needed to yield an unambiguous evidence for the predicted enhancement effect. Unfortunately, the temperature dependences of the effective relaxation rate T_{eff}^{-1} due to the static susceptibility and to the enhancement exhibit similar features; therefore, the separation of these two effects is difficult.

Finally, it should be noticed that the precise interpretation of the TESR data can be carried out only in terms of the dynamical susceptibility calculated in a microscopic way instead of the application of the phenomenological theory developed by Hasegawa[4] based on the Bloch equation. However, the theoretical study of the dynamical susceptibility is a very difficult task even for a simple s-d interaction neglecting any lattice relaxation process. Recently, for the latter case, the localized spin contribution to the dynamical susceptibility $\langle S^+(t) S^-(0) \rangle$ has been calculated with logarithmic accuracy,[23] while the other contributions are subjects for further investigations. Such a calculation of the dynamical susceptibility would answer the question whether the localized-spin–lattice relaxation contributes to the conduction-electron–lattice relaxation or not.

ACKNOWLEDGMENTS

We are grateful to Professor L. Pál for his continuous interest in this work. One of us (A. Zawadowski) is indebted to Professor Celli, Dr. J. Ruvalds, and Dr. P. Monod for useful discussions, and the staff of the Department of Physics at the University of Virginia for their hospitality.

FIG. 6. General form of the renormalized s-l vertex.

APPENDIX

The renormalization factor of $1/T_{sl}$ will be investigated in logarithmic approximation to any order in the s-d exchange interaction. The possible types of diagrams for the transition matrix elements are given in Fig. 6, where the full circle with one incoming and one outgoing electron line (see Fig. 7) is the renormalized vertex of the s-d exchange interaction. In the diagrams shown in Fig. 6 every possible time ordering of the interactions (including the spin-orbit interaction) must be taken into account. The contribution of the bare spin-orbit vertex is

$$-iB[(\vec{k}\times\vec{k}')^+/|\vec{k}\times\vec{k}'|]\, P_2^1(\cos\theta_{\vec{k}\vec{k}'}) . \tag{A1}$$

The calculation of the contribution of the diagrams given in Fig. 6 can be carried through in an approximation related to the solution of Suhl's equations[15] given by Brenig and Götze.[16] This solution contains all the highest-order logarithmic terms as well as a part of the lower-order ones. As it has been shown in Ref. 16, Suhl's equations are equivalent to the diagrammatical equation for the vertex Γ where only those diagrams have been considered which have no overlapping vertices, as shown by the diagrams in Fig. 8.

Let us start with the diagrams in Figs. 6(b) and 6(c) where the diagrams can be distinguished as (i) those without overlapping vertices in time, and (ii) others with overlapping vertices. The contribution of the diagrams of the type (i) can be calculated easily, and the result is similar to the one given by Eq. (12), only the value of the coupling constant J is replaced by the vertex function Γ. In this way we obtain

$$-iB\sum_{\vec{k}_1}\Gamma_{\uparrow,M,\uparrow M}(\epsilon_k;\vec{k},\vec{k}_1)\, G(\epsilon_{\vec{k}_1}) \times[(\vec{k}_1\times\vec{k}')^+/|\vec{k}_1\times\vec{k}'|]P_{\frac{1}{2}}^{\frac{1}{2}}(\cos\theta_{\vec{k}_1\vec{k}'}) , \tag{A2}$$

$$-iB\sum_{\vec{k}_1}[(\vec{k}\times\vec{k}_1)^+/|\vec{k}\times\vec{k}_1|]\, P_2^1(\cos\theta_{\vec{k}\vec{k}_1}) \times G(\epsilon_{\vec{k}_1})\,\Gamma_{\downarrow,M,\downarrow M}(\epsilon_{\vec{k}};\vec{k}_1,\vec{k}') \tag{A3}$$

corresponding to the diagrams in Figs. 6(b) and 6(c), respectively, and where $G(\epsilon)$ is given by Eq. (13).

A calculation of the transition probability due to

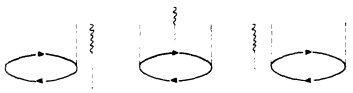

FIG. 7. Renormalized s-d vertex, with energy variable ϵ and momentum $\vec{k}$ and $\vec{k}'$.

the results given by Eqs. (A2) and (A3) shows that the term being linear in the real part of vertex functions vanishes (as has been found for the similar term of first order in the exchange coupling constant in Sec. III). This is a consequence of the fact that these contributions are purely imaginary. On the other hand, the term being linear in the imaginary part of the vertex yields contribution of the order $J^{n+2}\ln^n(D/T)$. The imaginary part of the vertex can be taken into account by replacing the single vertex by two subsequent real vertices shown in Figs. 9(a)–9(d)[24] where different time orderings are represented as well. According to Ref. 16, no overlapping between the vertices has to be considered (see the second and third diagrams in Fig. 8). In this way we can calculate the imaginary part of the vertex in logarithmic approximation, while the real contribution of vertex (represented now by two vertices) will be canceled as discussed above.

In order to treat the type (ii) of the diagrams in Figs. 6(b) and 6(c) where the generalized vertices and the bare electron-lattice vertex points overlap in time, the possible time orderings are shown in Figs. 9(e) and 9(f) where the original single vertex is cut into two parts (represented by two vertices) according to the position of the electron-lattice vertex point.

The class of those diagrams discussed above which contribute to the accuracy considered can be completed by the diagrams represented in Fig. 6(d), where the different time ordering must be taken into account. Furthermore, it can be shown, e.g., by studying the diagrams in third and fourth

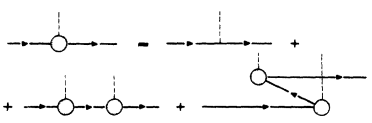

FIG. 8. Diagrams contributing to the Suhl's equations.

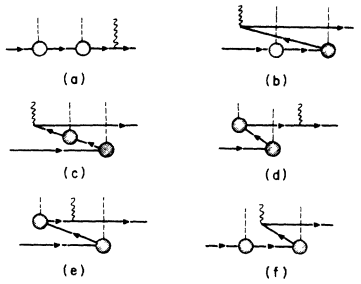

FIG. 9. Diagrams giving contributions in logarithmic approximation to the renormalization of the incoming electron lines in T_{sl}.

order in J, that the leading logarithmic contributions [terms proportional to $J^{n+2}\ln^n(D/T)$] come from the diagrams where there is no overlapping. The situation is similar to calculation of the renormalized vertex in Ref. 15 where the diagrams of the type represented in Fig. 8 yield the leading contributions in the logarithmic approximation.

In this way we obtained a class of diagrams containing two vertices (which are real in the logarithmic approximation). This class shows a one-to-one correspondence to the diagrams of second order which have been calculated in Sec. III. The diagram represented in Fig. 6(e) does not yield any contribution for the same reason that the diagram in Fig. 3(d) did not. It is of importance to notice that the calculation of the diagrams of second order in J shows that the kinetic energies of the intermediate electrons and holes are of the order of the thermal energy T or less. Therefore, the energy variable of the vertex function can be replaced by zero.

The considerations presented above can be summarized as follows: In the logarithmic approximation, the transition probability can be obtained from the results derived in Sec. III up to the second order in J by replacing the bare vertex by the vertex function in logarithmic approximation. This vertex function is[8]

$$\Gamma(0,\vec{k},\vec{k}') = 5P_2(\cos\theta_{\vec{k}\vec{k}'})\,\frac{J/N}{1+2\rho_0(J/N)\ln(D/T)}\ , \tag{A4}$$

where the d-type behavior of the scattering is taken into account. The final result is given by Eq. (15).

---

*Research supported in part by the Center for Advanced Studies at the University of Virginia, Charlottesville, Va. 22903.

†On leave from Central Research Institute for Physics, Budapest, Hungary.

[1]D. L. Cowan, Phys. Rev. Letters 18, 770 (1967).

[2]S. Schultz, M. R. Shanabarger, and P. M. Platzman, Phys. Rev. Letters 19, 749 (1967).

[3]P. Monod and S. Schultz, Phys. Rev. 173, 645 (1968).

[4]H. Hasegawa, Progr. Theoret. Phys. (Kyoto) 21, 483 (1959).

[5]Recently, Giovannini has shown that starting from the

Anderson model and then performing the Schrieffer-Wolff transformation (see Ref. 6) a conduction-electron–lattice relaxation may contribute to the localized-moment-lattice relaxation in the transformed Hamiltonian (unpublished).

[6]R. J. Schrieffer and P. A. Wolff, Phys. Rev. 149, 491 (1966).

[7]J. Kondo, Progr. Theoret. Phys. (Kyoto) 28, 846 (1962).

[8]The assumption made here is in agreement with the result of Ref. 6.

[9]L. D. Landau and E. M. Lifshitz, *Quantum Mechanics* (Pergamon, New York, 1965).

[10]The application of Feynman diagrams to spin-dependent interactions is not generally justified owing to the different spin factors for the different time-ordered diagrams. In second order in H_{sd} and without external magnetic field, the spin factors for the different time-ordered diagrams are the same, and therefore Feynman diagrams can be used. In the presence of a strong external magnetic field, however, where $\langle M \rangle$ cannot be neglected compared to $S(S+1)$, even in second order in H_{sd} Feynman diagrams cannot be applied.

[11]Further discussion of this approximation can be found in the Appendix of Ref. 13.

[12]A. A. Abrikosov, Physics 2, 5 (1965).

[13]F. Mezei and A. Zawadowski (unpublished).

[14]J. Sólyom and A. Zawadowski, Physik Kondensierten Materie 7, 325 (1968); 1, 342 (1968).

[15]H. Suhl, Phys. Rev. 138, A515 (1965).

[16]W. Brenig and W. Götze, Z. Physik 217, 188 (1969).

[17]A. Zawadowski and P. Fazekas, Z. Physik 226, 235 (1969).

[18]See Eqs. (18) and (24).

[19]A. Zawadowski and P. Fazekas, J. Appl. Phys. (to be published).

[20]M. D. Daybell and W. A. Steyert, Phys. Rev. Letters 20, 195 (1968).

[21]M. D. Daybell, W. P. Pratt, Jr., and W. A. Steyert, Phys. Rev. Letters 22, 401 (1969).

[22]P. Fazekas and A. Zawadowski (unpublished).

[23]The definition of T_{eff} can be found in Refs. 3 and 4.

[24]This result is proved by Abrikosov (see Ref. 12) and corresponds to a unitarity condition.

PHYSICAL REVIEW B VOLUME 3, NUMBER 1 1 JANUARY 1971

Raman Scattering in $CsMnF_3$ †

S. R. Chinn

Lincoln Laboratory, Massachusetts Institute of Technology, Lexington, Massachusetts 02173

(Received 17 August 1970)

We have observed Raman scattering from the antiferromagnet $CsMnF_3$ over the temperature range from 5 to 300 °K. Of the 33 predicted Raman active normal modes, at low temperature, we have observed and identified 29, belonging to the A_{1g}, E_{1g}, and E_{2g} representations of the space group D_{6h}^4. At higher temperatures many of these lines broadened and shifted in energy from anharmonic interactions. Below the antiferromagnetic ordering temperature 53.5 °K, we have also seen Raman scattering from a two-magnon excitation located at 92.8 cm^{-1} at 5 °K. The energy of this line is consistent with the prediction of spin-wave modes calculated using previously determined excnange constants.

I. INTRODUCTION

The compound $CsMnF_3$ is a transparent antiferromagnet ($T_N = 53.5$ °K)[1] which belongs to the hexagonal space group D_{6h}^4. In this structure, shown in Fig. 1, there are 30 atoms or six formula units in the unit cell in both the paramagnetic and antiferromagnetic phases. This compound is different in its structure and properties from the chemically similar perovskites such as $RbMnF_3$ and $KMnF_3$, and is isomorphic with $RbNiF_3$ and the hexagonal modification of $BaTiO_3$. Much recent work, particularly concerning the magnetic and optical properties, has been carried on $CsMnF_3$, including NMR,[1–4] optical absorption,[5,6] and magnetoelastic interaction studies.[7] This paper reports on phonon and two-magnon excitations which were observed in $CsMnF_3$ by means of Raman scattering.

Before continuing with the results of the present experiment and their interpretation, we shall briefly summarize the most important features of the $CsMnF_3$ structure. In their antiferromagnetically ordered state, the spins of the Mn^{2+} ions ($S=\frac{5}{2}$) lie in the basal plane in alternate antiparallel layers.[1] In addition to the negative uniaxial anisotropy, there is also a very small basal plane anisotropy having sixfold symmetry. Examination of the crystal structure shows that there are two different types of sites for the Mn^{2+} ions. One type, labeled A, is in a slightly distorted octahedron of F^- ions which shares only corners with other $6F^-$-Mn^{2+} octahedra. The second type of site, labeled B, is in an octahedron which shares three corners with A-site octahedra and a common face with another B-site octahedron. As in $RbNiF_3$,[8] this structure gives rise to two types of superexchange paths, one with an approximately 180° angle, for the Mn_A-F-Mn_B bond, and the other, about 90°, for the Mn_B-F-Mn_B bond. In $CsMnF_3$, both of these interactions are antiferromagnetic.